

# Study of Tribological Characteristics of Grooved and Flat Surfaces Using Inclined Slider Bearings

Muhannad Mohsen Mrah and Ammar S. Hamid Merza

Mechanical Engineering Department, University of Technology, Baghdad-Iraq.

**Abstract** - This research aims to determine how surface grooves affect the lubrication mechanism in an inclined Slider bearing. Reynolds' equation was used in theory to calculate the pressure gradient in a one-dimensional fluid film. The experiment results were studied by the tilted sliding bearing, where the researcher manufactured and developed the device by adding sensors along the pad to read the pressure distribution in each pad. Four pads were manufactured, one without grooves and three with rectangular grooves. Numerous variables were investigated in this study, including sliding velocities, pad inclination values, and oil temperatures. The conclusions indicate that the flat model is significantly superior to the grooved models. The maximum load-carrying capacity of flat and groove models was in the film ratio ( $K$ ) = 2. The present and previous work have been compared experimentally (just in behaviors). The sample used in this comparison was flat; the results indicated that the sensors provided higher pressure levels than the manometer tubes under the same operating conditions.

**Index Terms** - load-carrying capacity, pressure distribution, surface grooves, thrust bearing.

## INTRODUCTION

Every second of every day, machines worldwide are churning out the products we require. These machines rely on the bearings' successful support. The wide range of mechanical applications with interacting surfaces and increased industrial competition for improved performance and more cost-effective products has led to increased attention to research in the science of friction, wear, and lubrication, i.e., tribology [1]. Many machine components, e.g., bearings, gears, piston rings, and breaks, consist of parts that operate by rubbing against each other [2]. With extensive applications of slider bearings in mechanical devices, investigations associated with their design and performance optimization have been given privilege. Current industrial requirements include increased load-carrying capacity, lower friction, and lower power consumption. To increase the performance of the bearing in different machine elements during lubrication, e.g., slider bearings and roller bearings, it is essential to find the optimum design of slider bearings such as plane surfaces, step, composite, inclined, curved, cycloidal, and polynomial (by using different shapes of pad surfaces). In this research, slider bearings with various shapes of pads are investigated experimentally. Slider bearings are widely used in engineering applications such as mechanical seals, machine tools, steam turbines, gas turbines, piston rings, etc. (for their load-carrying capacity, excellent stability, and durability) [3]. Some workers analyzed slider bearings for different purposes using numerical techniques, treating the analyzed film thickness as the slider bearing shape function. So, manufacturing a slider bearing shape is sometimes challenging to match with the numerical shape, so the approach shape function can be obtained using curve fitting techniques. However, there is inevitably some error between the numerical shape and the curve-fitting shape function.

Recently, surface texturing has been used to improve the tribological characteristics of mechanical components. Texturing a surface can be advantageous in a variety of ways. For example, it can reduce friction and wear, increase load carrying capacity, and increase fluid film stiffness [4-6]. Generally, the primary functions of surface texturing are to control adhesion and stiction [7], to provide reservoirs for improved lubricant retention [8], and to generate hydrodynamic pressure to increase load-carrying capacity [9],[10], among others. With these capabilities, it is not surprising that surface texturing is widely used in various fields, including thrust bearings [11]–[13] and journal bearings [14],[15].

The previous scientific literature that discusses the combined effects of pad surface profile and pad geometry assumes flat pads with no rectangular slots in the surfaces. The goal of reducing friction and the desire to get the highest load capacity in the operating conditions of tilting-pad thrust bearings resulted in the following research question: is it possible to achieve performance improvements, i.e., a lower friction coefficient and higher load-carrying capacity, by applying features like rectangular slots to the surfaces of the bearing pads? The shape of sliding bearings is subject to many considerations. Usually, bearing designers try to select design variables within work constraints through trial and error methods, using design schemes resulting from analysis of bearing characteristics. This method often produces unconvincing results and does not give the optimal design solution. Thus, the optimal design of sliding bearing shapes has become an essential and exciting topic in recent years. In this research, it is essential to obtain the optimal shape of inclined bearings that meets the desired ambition of obtaining the highest load capacity and the lowest friction, thus obtaining the lowest energy consumption in the machine during lubrication.

In this research, it is essential to obtain the optimal shape of inclined bearings that meets the desired ambition of obtaining the highest load capacity and the lowest friction, thus obtaining the lowest energy consumption in the machine during lubrication.

## EXPERIMENTAL APPARATUS

The system consists of a plane aluminum slider, 12.5cm<sup>2</sup>; Dimensions are placed precisely in proportion to the movable belt, which carries a thick oil film. Figure 1. shows a diagram of the device used, consisting of two rotating cylinders (A, B) connected by an oil conveyor belt. The cylinder (A) is driven by an electric motor through which the cylinder rotation speed can be

controlled and thus the linear velocity of the conveyor belt. Models with the exact dimensions as the slider but a thickness of 4 mm can be installed in the lower area of the slider. It contains pressure gauge holes attached to it, plastic tubes that transfer the oil pressure to the sensors to measure the oil pressure inside the sample, and these tubes are longitudinally distributed. To calculate the change in pressure resulting from the trapping of oil between the moving belt and the model tilted at a certain angle and cross tubes to indicate the balance and level of the device, the oil flows from (C) to region (D). The clearance between the belt and the sample is controlled by a micrometer at the edge (C, D), and the device is placed in a basin, part of which is filled with oil.

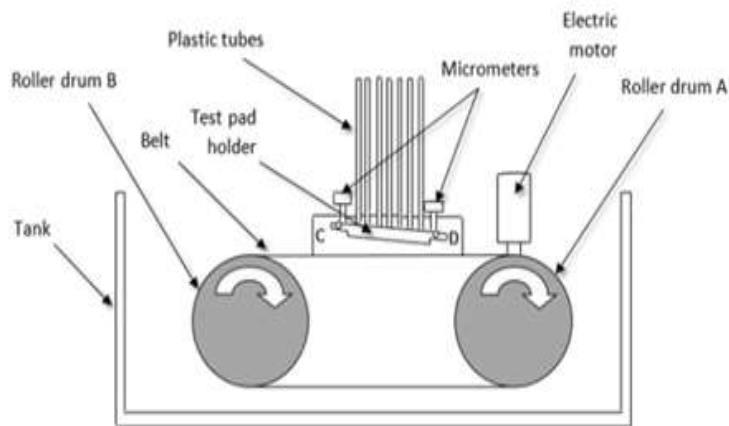


FIGURE 1  
SCHEMATIC OF THE EXPERIMENTAL APPARATUS.

The clearance between the slider and the belt is determined using two micrometers. They are parallel to the slider's leading and trailing edges. One of these micrometers was attached to the leading edge and the other to the trailing edge. Thirteen sensors attached to the slider provide information about the amount of oil pressure generated by the slider and the moving belt via plastic tubes. Seven of these sensors are evenly spaced in the direction of movement along the slider's axis. Simultaneously, another group is transversely located in a plane roughly parallel to the expected location of the oil's maximum pressure [16]. Figure 2 illustrates the devices used in conjunction with the additional instruments.

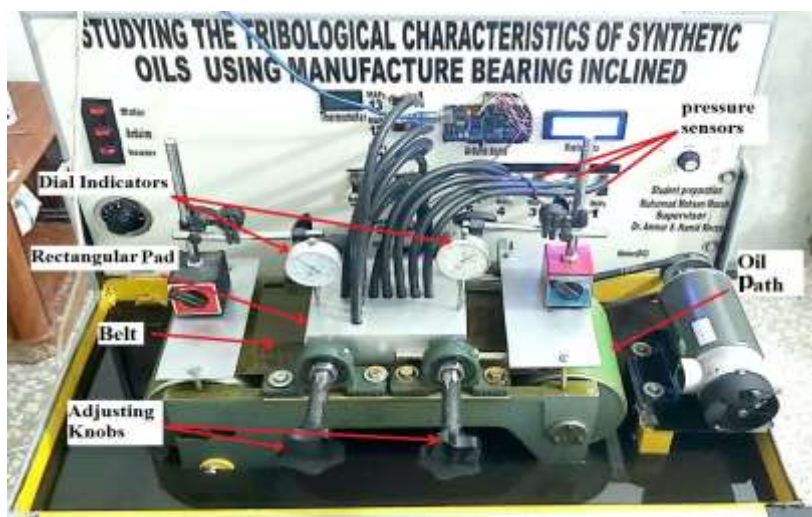


FIGURE 2  
THE TILTING-PAD BEARING TEST RIG.

#### MATERIALS

Aluminum was used as the metal for the produced models; the thickness of the manufactured models is 4mm. This metal was chosen for its availability and simplicity of installation on the equipment. The metal was chopped into squares (12.5cm<sup>2</sup>) to match the models (4). A CNC machine was used to create rectangular grooves on the models. Four pads were manufactured, one without slots and three with rectangular grooves (orienting the grooves in the direction of the oil flow) and varying slot widths (3, 5, and 8mm) and a depth of 2mm, as shown in figure 3. The models must be identical in size to the holes in the equipment used, have the same diameter, and have the same number of holes (13). These holes are placed next to the pad's holes to allow oil to flow through the pipes to measure the oil pressure.



FIGURE 3  
FLAT AND SLOTS MODELS.

### METHOD

The Reynolds equation describes the change of lubricating pressure in a bearing. The most popular lubricated slider bearing is the inclined plane pad, which demonstrates how the Reynolds equation may be used for slider bearings (where this type has been studied in this research). The complete equation is complicated to solve. Still, a reduced form will be utilized in the first instance by making several derivational assumptions and using the equilibrium of a tiny element to derive the Reynolds equation in one dimension [17]. The following equation was developed to express the change in pressure along a converging fluid film in terms of the velocity gradient across the film:

$$\frac{dP}{dx} = \eta \frac{d^2u}{dy^2} \quad (1)$$

$$\text{or } \frac{d^2u}{dy^2} = \frac{1}{\eta} \frac{dP}{dx} \quad (2)$$

Integrating (2) twice with respect to  $y$  gives:

$$\frac{du}{dy} = \int \frac{1}{\eta} \frac{dP}{dx} dy = \frac{1}{\eta} \frac{dP}{dx} y + C_1$$

And

$$u = \int \frac{1}{\eta} \frac{dP}{dx} y dy + C_1 dy = \frac{1}{2\eta} \frac{dP}{dx} y^2 + C_1 y + C_2 \quad (3)$$

The constants of integration  $C_1$  and  $C_2$  may be evaluated from the boundary conditions:

1.  $u = U$  when  $y = 0$
2.  $u = 0$  when  $y = h$

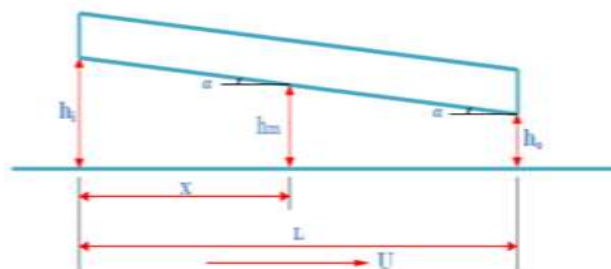


FIGURE 4  
GEOMETRY OF A LINEAR PAD BEARING.

From condition (1) it follows that  $C_2 = U$  and from condition (2)

$$C_1 = -\frac{1}{2\eta} \frac{dP}{dx} h - \frac{U}{h}$$

By introducing the values of these constants into (3), it becomes:

$$u = \frac{1}{2\eta} \frac{dP}{dx} (y^2 - hy) + U \frac{h-y}{h} \quad (4)$$

The first component in the right-hand member of (4) denotes a parabolic distribution of velocity caused by the pressure-driven flow in the film. The second component in (4) right-hand member illustrates a linear distribution of velocity caused by the relative motion of the two surfaces. Now we need to find an expression for the volume of fluid flowing through the bearing [18]. By using the above assumptions and defining (Q) as the volume of fluid flowing in a unit of time,

$$Q = \int_0^h u \, dy$$

By substituting the value of u from (4) and integrating, the equation for (Q) becomes,

$$Q = \frac{Uh}{2} - \frac{h^3}{12\eta} \frac{dP}{dx}$$

For an incompressible fluid, the flow is the same for all cross sections of the film, or

$$\frac{dQ}{dx} = 0$$

Therefore,

$$\frac{dQ}{dx} = \frac{U}{2} \frac{dh}{dx} - \frac{d}{dx} \left( \frac{h^3}{12\eta} \frac{dP}{dx} \right) = 0$$

$$\frac{d}{dx} \left( h^3 \frac{dP}{dx} \right) = 6\eta U \frac{dh}{dx} \quad (5)$$

This is the one-dimensional Reynolds' equation for the pressure gradient in a converging fluid film, which is ignored by side leakage (flow in the z-direction).

### *I. Pressure and load capacity distributions*

By integrating (5) twice with respect to x gives:

$$P = \frac{6\eta UL}{h_0^2} \left( \frac{K-1}{K+1} \frac{\frac{X}{L} (1 - \frac{X}{L})}{[K - (K-1) \frac{X}{L}]^2} \right) \quad (6)$$

Further integration of (6) yields the sliding bearing's normal load capacity per unit width [17]:

$$\frac{W}{B} = \int_{x=0}^{x=L} P \, dx \quad (7)$$

The load bearing capacity equation becomes:

$$W = \frac{6\eta UL^2 B}{h_0^2} \frac{1}{(K-1)^2} \left( \log_e K - \frac{2(K-1)}{K+1} \right) \quad (8)$$

## II. Shear Stress In Hydrodynamic Film

To evaluate the shear stress along the length of the bearing at the lower surface, the definition of Newtonian viscosity and (4) is used to get:

$$\tau_o = -\frac{h}{2} \frac{dP}{dx} - \frac{\eta U}{h} \quad (9)$$

Also, the shear stress at the upper surface:

$$\tau_h = \frac{h}{2} \frac{dP}{dx} - \frac{\eta U}{h} \quad (10)$$

## III. Friction force

Friction is the resistance to motion that exists between two solid bodies as one slides over the other. The resistive force perpendicular to the direction of motion is referred to as the "friction force" Even such negligible frictional forces result in energy waste and subsequent loss of machine efficiency. As a result, the designer's goal is often to minimize frictional forces. The frictional force is calculated using the following equation:

$$F = \int_0^L \tau \, dx \quad (11)$$

The friction force on the lower surface is

$$F_o = \frac{\eta U L B}{h_o} \left[ \frac{4 \log_e K}{K-1} - \frac{6}{K+1} \right] \quad (12)$$

$$F_h = \frac{\eta U L B}{h_o} \left[ \frac{2 \log_e K}{K-1} - \frac{6}{K+1} \right] \quad (13)$$

## IV. Coefficient of friction

As it is known that

$$\mu = \frac{F}{W} \quad (14)$$

Substituting for W and F and simplification the above equation yields:

$$\mu = \frac{h_o}{L} (K-1) \left[ \frac{2(K+1) \log_e K - 3(K-1)}{3(K+1) \log_e K - 6(K-1)} \right] \quad (15)$$

## EXPERIMENTAL CALCULATIONS

The seven pressure sensors were tested with a constant belt speed for a range of film ratios, with the film thickness  $h_o$  at the trailing edge remaining constant while the film thickness  $h_o$  at the leading edge was gradually increased. The following are the corresponding calculations for a few of these tests:

TABLE I  
LIST OF PARAMETERS USED IN EXPERIMENTAL CALCULATIONS

models	flat
Type oil	Bright stock
temperature	35 °C
Film ratio K (hi / ho)	2
Pad length (L)	0.125 m
Belt length	1.25 m
Sliding velocity	0.1 m/s
Density	900 kg/m <sup>3</sup>
Viscosity of oil at T=35 °C	395 cSt

Generally, kinematic viscosity is expressed in centistokes; the relationship between viscosity ( $\eta$ ) expressed in centistokes and in SI units is as follows:

$$\nu = (\text{cSt}) \times 10^{-6} \quad \text{m}^2/\text{s}$$

Given that kinematic viscosity is defined as (viscosity)/(density), the following may be written:

$$\eta = \rho \nu = \rho (\text{cSt}) 10^{-6} \quad \text{kg/ms}$$

a) The Pressure was calculated by using the (6).

$$P = \frac{6 \eta U L}{h_0^2} \left( \frac{K-1}{K+1} \frac{\frac{X}{L} (1 - \frac{X}{L})}{[K - (K-1) \frac{X}{L}]^2} \right)$$

TABLE II  
LIST OF SIMPLE CALCULATIONS

station	1	2	3	4	5	6	7
P(practical) pa	290	886	1793	2657	2995	3840	3860
P(theoretical)pa	329	985	1943	2827	3565	4060	4005

**Note:** Through the above table, it is possible to calculate the error rate between the theoretical and experimental parts, as the error rate is estimated at about 10%. The presence of such a percentage is due to the natural leakage of oil from both sides of the pad, in addition to the vibrations emanating from the motor, as well as the design of the pad (roughness and texture).

b) The load capacity was calculated by using the (8).

$$W = \frac{6 \eta U L^2 B}{h_0^2} \frac{1}{(K-1)^2} \left( \log_e K - \frac{2(K-1)}{K+1} \right)$$

$$W = \frac{6 * 0.33 * 0.1 * (0.125)^2 * 0.125}{(0.0005)^2} \frac{1}{(2-1)^2} \left( \log_e 2 - \frac{2(2-1)}{2+1} \right)$$

$$W = 40.962 \text{ N}$$

c) The coefficient of friction was calculated by using (15).

$$\mu = \frac{h_o}{L} (K - 1) \left[ \frac{2(K + 1) \log_e K - 3(K - 1)}{3(K + 1) \log_e K - 6(K - 1)} \right]$$

$$\mu = \frac{0.0005}{0.125} (2 - 1) \left[ \frac{2(2 + 1) \log_e 2 - 3(2 - 1)}{3(2 + 1) \log_e 2 - 6(2 - 1)} \right]$$

$$\mu = 0.01945 [19]$$

## RESULTS AND DISCUSSION

### I. Effect of Sliding speeds on the load-carrying capacity

Figure 5 show the relationship between the load-carrying capacity (W) and the sliding velocity of the oil for grooved models compared with the flat model. It is evident from the figures that the P mean is directly proportional to the sliding speed. Whereas as the belt speed increases (the speed of the oil slip), the amount of oil trapped between the belt and the cushion increases, increasing the P mean inside the tubes and thus the sensors' reading for the flat model. As for the slots models, they are constructed similarly to the flat models, except that the distance between the belt and the cushion will be greater due to the presence of slots that require a more significant amount of oil to fill. Because the flow is constant, the average pressure of the flat model will be greater than the average pressure of the slots models. When the sliding velocity (which is directly proportional to the load-carrying capacity in (8)) has been increased, the P mean (which is also directly proportional to the load-carrying capacity) will also increase. For this reason, the load-carrying capacity will increase at various sliding velocities. As we have noted in the previous figures, the average pressure of the flat model is higher than the average pressure in the groove models, and therefore the loading capacity of the flat model is higher than the other models.

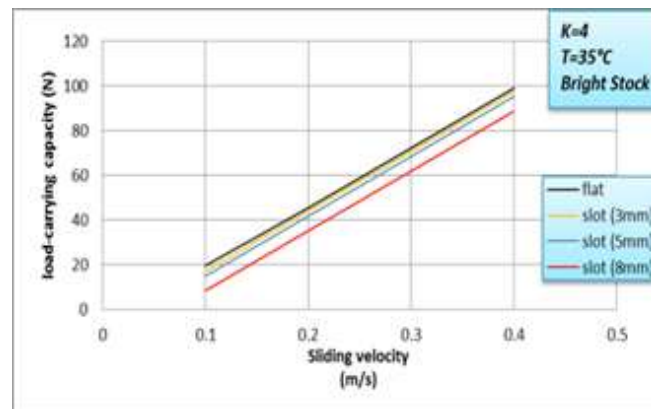


FIGURE 5

RELATION BETWEEN LOAD CAPACITY AND SLIDING VELOCITY

### II. Effect of temperature on the load carrying capacity

The relationship between oil temperature and the load-carrying capacity is depicted in Figure 6. As shown in the figure, as the temperature of the oil increases, the load-carrying capacity decreases (inversely proportional). As the temperature increases, the forces between the oil molecules weaken and move away from one another, causing the liquid to expand and thus reduce its viscosity. When the viscosity of the oil decreases and the flow velocity remains constant, the amount of oil trapped between the belt and the cushion decreases, lowering the p mean (directly related to load-carrying capacity) for each model. As previously explained, the slots increase the volume enclosed between the cushion and the belt, requiring a more significant amount of oil.

■ P mean (flat plat > slot 3mm > slot 5mm > slot 8mm).

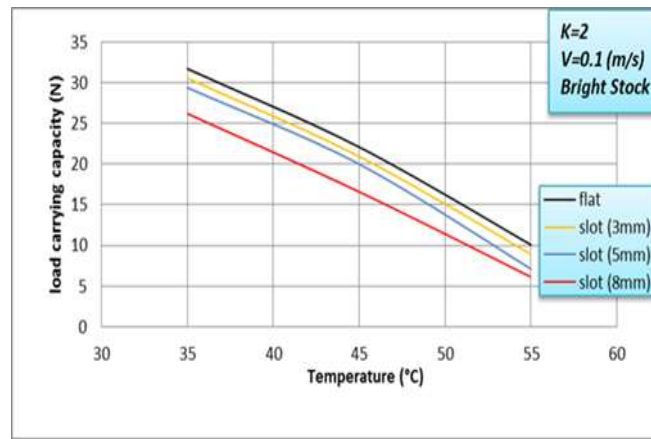


FIGURE 6

RELATION BETWEEN LOAD CAPACITY AND TEMPERATURE.

### III. Effect of an inclination on the load-carrying capacity

The relationship between the inclination of the pad and the load-carrying capacity is depicted in Figure 7. We observe that as the inclination increases, the load-carrying capacity decreases (inverse proportion). This is because the higher the inclination value, the more volume is constrained between the pad and the belt. As a result, the oil pressure is reduced (constant flow rate) in comparison to the flat pad. In the case of grooved pads, the presence of grooves increases the value of  $K$ , resulting in a more significant decrease in pressure. When the value of ( $K$ ) is (2), the maximum increase in ( $W$ ) occurs, and then the value of ( $W$ ) steadily decreases as the value of ( $K$ ) increases. This is more accurate than what Gropper et al. recommended in their review (The highest load capacity is obtained whenever the value of the inclination of the cushion is close to zero) [20].

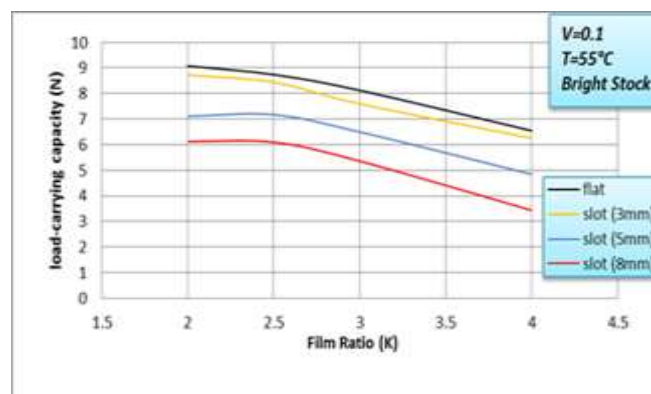


FIGURE 7

RELATION BETWEEN LOAD CAPACITY AND FILM RATIO.

### IV. Effect of sliding speeds on the coefficient of friction

Figure 8 show the relationship between slip speed and the coefficient of friction. In general, when the sliding speed increases, the coefficient of friction decreases (an inverse relationship) since when the sliding speed increases, the load-carrying capacity will also increase, which is inversely proportional to the friction coefficient in (14). When the surface is flat, the load capacity will be higher than that of the grooved surfaces, and thus the lowest coefficient of friction will be obtained. Whereas, when the surface is grooved, the load capacity will be less than the flat surface [ $W_{\text{slot 3mm}} > W_{\text{slot 5mm}} > W_{\text{slot 8mm}}$ ] and thus, you will get the highest coefficient of friction. We note that the coefficient of friction for all surfaces is at its maximum when the sliding speed is low, and the reason for this is that the load capacity is very low compared to the friction force that occurs between the oil and the belt.

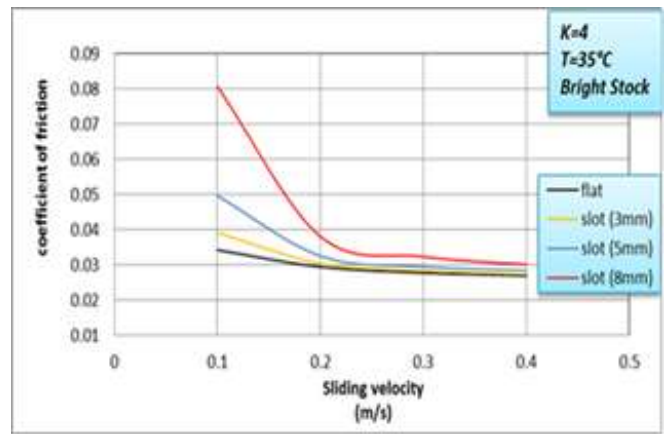
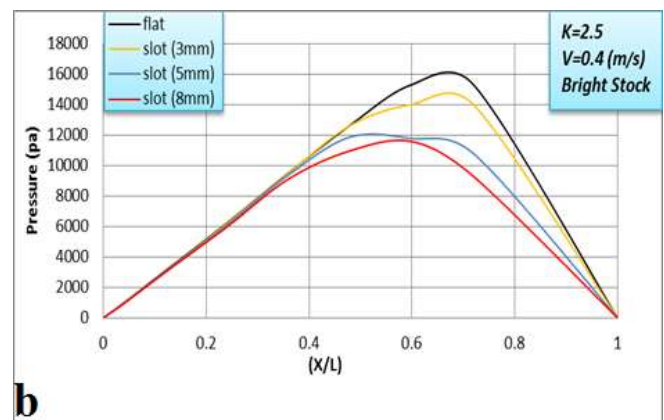
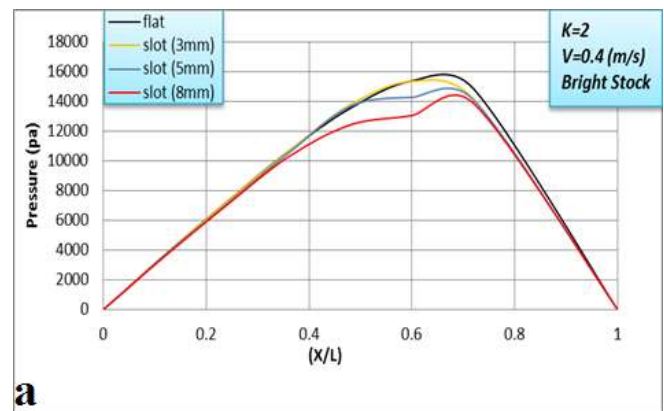


FIGURE 8

RELATION BETWEEN COEFFICIENT OF FRICTION AND SLIDING VELOCITY.

V. Pressure distribution along the pad

The figure (9a-d) depict the relationship between the pressure at any location on the pad's surface and the proportion between ( $X/L$ ) for grooved models and flat ones. The pressure value begins at zero at the pad's leading-edge and steadily grows throughout the pad's length until it reaches its maximum value in the pad's back half (where the fluid adhering to the moving surface will be dragged into the narrowing clearance space, thus building up a pressure sufficient to carry the load). The pressure value will then decline until it hits zero at the pad's trailing edge.



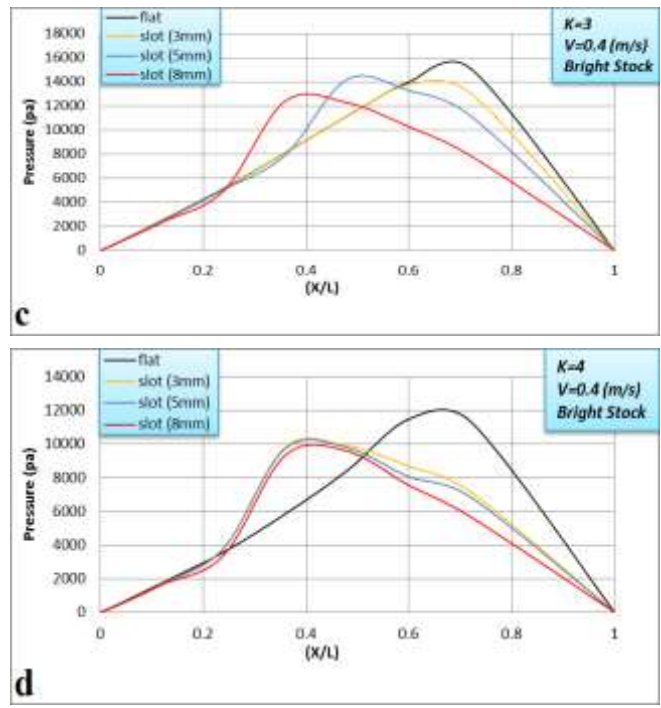


FIGURE 9A-C  
 PRESSURE DISTRIBUTION FOR ALL MODELS AT T=35°C.

As illustrated in Figures (9c-d), flat pads provide the highest average pressure of the other models. This is because the distance between the pad and the belt is smaller for the flat surface model than it is for the other models, implying that the confined fluid volume is smaller. One important point to note is that, as the value of K increases, the maximum average pressure of the groove pads begins to approach the center of the pad. This is because the grooves increase the surface friction, which works to return the maximum pressure to the center of the pad approximately.

Figure 10 illustrates the nondimensional oil film thickness distribution in the circumferential direction for the centerline and outer arc. It is obvious that the amount of pressure production in the oil film varies along the circumferential direction. The pressure on the pad surface is minimal on the sides of the edge; nevertheless, a significant amount of pressure is generated on the pad surface at the trailing edge. Because the peak pressure is somewhat towards the trailing edge, the maximum pressure values are situated closer to the trailing edge.

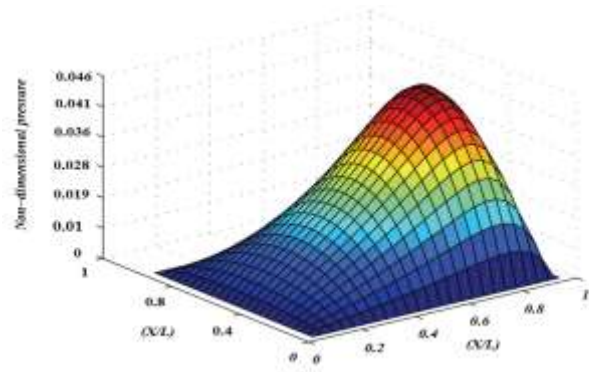


FIGURE 10  
 NON-DIMENSIONAL PRESSURE DISTRIBUTION WITH AND CIRCUMFERENTIAL DIRECTION.

VI. Comparison between the present work and the previous work

The current work was compared to previous work [21]. This comparison used a flat sample. Pressure sensors [22] were used in the current work, whereas manometer tubes were used in the previous work. As illustrated in Figure 11, the pressure distribution at the current work is higher than it was at the previous work (but with the same behavior). This is because the sensors take direct readings from the bottom of the pad's surface. In previous work, readings were taken by observing the liquid level inside the manometer tubes, as the liquid inside the tubes has a different density than the liquid beneath the pad's surface due to the

temperature difference. Between the oil and the surroundings, Since temperature differences affect fluid density, most of the research concerned with studying the pressure distribution in a sliding inclined bearing should pay close attention to this factor.

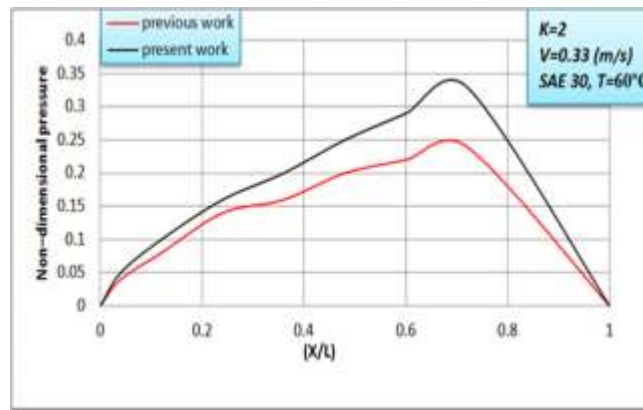


FIGURE 11

COMPARISON BETWEEN THE PRESENT WORK AND THE PREVIOUS WORK.

### CONCLUSIONS

According to the analysis of the findings, the following conclusions may be drawn from the present work:

1. When a flat model is used instead of a groove model, the pressure distribution is improved for the same operating circumstances.
2. For grooves models, the pressure distribution has been increased at ( groove width of 3mm) more than the increase at (groove width of 5mm and 8mm).
3. The flat model's coefficient of friction is lower than the coefficient of friction of the groove models, with percentages of 0.38%, 4.63%, and 17.37%, respectively.
4. The maximum load-carrying capacity of flat and groove models was in the film ratio (K) of 2 to 2.5., whereas the load capacity of the flat model was more significant than the load-carrying capacity of the groove models by percentages of 0.5%, 4.27%, and 14.66%, respectively.
5. Pressure distribution has been improved when the belt speed has been raised, irrespective of the test model.
6. One significant conclusion for models with grooves is that as the inclination increases, the maximum load capacity approaches the center of the pad, allowing grooves models to be used in applications requiring less load and weight.

### NOMENCLATURE

Symbol	Description	Unit
B	Pad width	m
C, C <sub>1</sub> , C <sub>2</sub>	Integration constants	---
F	Friction force	N
h	Film thickness	m
h <sub>i</sub>	Film thickness, leading edge	m
h <sub>o</sub>	Film thickness, trailing edge	m
h <sub>m</sub>	Maximum height when dp/dx = 0	m
K	Film ratio h <sub>i</sub> / h <sub>o</sub>	---
L	Pad length	m
P	Pressure	N/m <sup>2</sup>
Q	Lubricant flow rate	m <sup>3</sup> /s
T	Temperature	C°
u, U, V	Sliding velocity	m/s
W	Load carrying capacity	N
η	Dynamic viscosity	Kg/m.s
τ	Shear stress	N/m <sup>2</sup>

## ACKNOWLEDGMENT

I would like to acknowledge Dr. Shaker Sakran Hassan (the support is gratefully acknowledged). I also would like to acknowledge the staff of Mechanical Engineering Department / University of Technology and the people who helped me (thank you very much).

## References

- [1] G. W. Stachowiak, "How tribology has been helping us to advance and to survive," *Friction*, vol. 5, no. 3, pp. 233–247, 2017, doi: 10.1007/s40544-017-0173-7.
- [2] C. Gu, X. Meng, S. Wang, and X. Ding, "Study on the mutual influence of surface roughness and texture features of rough-textured surfaces on the tribological properties," *Proc. Inst. Mech. Eng. Part J J. Eng. Tribol.*, vol. 235, no. 2, pp. 256–273, 2021, doi: 10.1177/1350650120940211.
- [3] A. Arslan *et al.*, "Surface Texture Manufacturing Techniques and Tribological Effect of Surface Texturing on Cutting Tool Performance: A Review," *Crit. Rev. Solid State Mater. Sci.*, vol. 41, no. 6, pp. 447–481, 2016, doi: 10.1080/10408436.2016.1186597.
- [4] J. Bouyer, M. Wodtke, and M. Fillon, "Experimental research on a hydrodynamic thrust bearing with hydrostatic lift pockets: Influence of lubrication modes on bearing performance," *Tribol. Int.*, vol. 165, no. September 2021, p. 107253, 2022, doi: 10.1016/j.triboint.2021.107253.
- [5] X. Zhang, G. Gao, Z. Yin, Y. Wang, and C. Gao, "Numerical analysis and experimental research on load carrying capacity of water-lubricated tilting-pad thrust bearings," *Mech. Ind.*, vol. 19, no. 2, pp. 22–24, 2018, doi: 10.1051/meca/2018005.
- [6] A. Erdemir, "Review of engineered tribological interfaces for improved boundary lubrication," *Tribol. Int.*, vol. 38, no. 3, pp. 249–256, 2005, doi: 10.1016/j.triboint.2005.08.008.
- [7] B. Bhushan, "Adhesion and stiction: Mechanisms, measurement techniques, and methods for reduction," *J. Vac. Sci. Technol. B Microelectron. Nanom. Struct.*, vol. 21, no. 6, p. 2262, 2003, doi: 10.1116/1.1627336.
- [8] H. Yu, X. Wang, and F. Zhou, "Geometric shape effects of surface texture on the generation of hydrodynamic pressure between conformal contacting surfaces," *Tribol. Lett.*, vol. 37, no. 2, pp. 123–130, 2010, doi: 10.1007/s11249-009-9497-4.
- [9] K. Yagi, H. Sato, and J. Sugimura, "On the magnitude of load-carrying capacity of textured surfaces in hydrodynamic lubrication," *Tribol. Online*, vol. 10, no. 3, pp. 232–245, 2015, doi: 10.2474/trol.10.232.
- [10] Kumar, M., Tyagi, R. Tribological Performance of Bearing Steel with Bi-triangular and Circular Textures under Lubricated Sliding. *J. of Materi Eng and Perform* (2022). <https://doi.org/10.1007/s11665-021-06568-5>
- [11] Y. Wang, Y. Liu, Z. Wang, and Y. Wang, "Surface roughness characteristics effects on fluid load capability of tilt pad thrust bearings with water lubrication," *Friction*, vol. 5, no. 4, pp. 392–401, 2017, doi: 10.1007/s40544-017-0153-y.
- [12] D. Gropper, T. J. Harvey, and L. Wang, "Numerical analysis and optimization of surface textures for a tilting pad thrust bearing," *Tribol. Int.*, vol. 124, pp. 134–144, 2018, doi: 10.1016/j.triboint.2018.03.034.
- [13] Zhang, Xiaohan "An Analysis of Surface Roughness and its Influence on a Thrust Bearing," *J. Phys. Ther. Sci.*, vol. 9, no. 1, pp. 1–11, 2018, [Online]. doi.org/10.1016/j.humov.2018.08.006.
- [14] K. Maharshi, T. Mukhopadhyay, B. Roy, L. Roy, and S. Dey, "Stochastic dynamic behaviour of hydrodynamic journal bearings including the effect of surface roughness," *Int. J. Mech. Sci.*, vol. 142–143, pp. 370–383, 2018, doi: 10.1016/j.ijmecsci.2018.04.012.
- [15] Benti, G. B., Rondon, D., Gustavsson, R., and Aidanpää, J. (August 24, 2021). "Numerical and Experimental Study on the Dynamic Bearing Properties of a Four-Pad and Eight-Pad Tilting Pad Journal Bearings in a Vertical Rotor." *ASME. J. Energy Resour. Technol.* January 2022; 144(1): 011304. <https://doi.org/10.1115/1.4052032>
- [16] Kingsbury Inc., "A general guide to the principles, operation and troubleshooting of hydrodynamic bearings," 2019.
- [17] Gwidon Stachowiak ,Andrew Batchelor, " Engineering Tribology 4th Edition". ISBN: 9780128100318. Butterworth Heinemann. September 2013.
- [18] J. Halling, " Principles of Tribology " , Published by the Macmillan Press Limited, London and Basingstoke, 1978, P. 233, 235, 239, 242.
- [19] Muhannad M. Mrah " Studying The Tribological Characteristics Of Synthetic Oils Using Manufactured Inclined Bearing". Thesis, University of Technology, Iraq, 2022.
- [20] D. Gropper, L. Wang, and T. J. Harvey, "Hydrodynamic lubrication of textured surfaces: A review of modeling techniques and key findings," *Tribol. Int.*, vol. 94, pp. 509–529, 2016, doi: 10.1016/j.triboint.2015.10.009.
- [21] Yasir Akram Abd Al - Rida, " Study the Influence of the Triangular Slots on the Lubrication Characteristics in the Inclined Slider Bearing " , Master thesis, University of Technology, Department of Mechanical Engineering, 2011.
- [22] E-radionica.com, "Pressure Sensor MPS20N0040D-S\_datasheet," pp. 13, [Online]. Available: <https://datasheet4u.com/datasheet-pdf/ETC/MPS20N0040D-S/pdf.php?id=996460>.